PAPER • OPEN ACCESS

Cross-comparative analysis of loads and power of pitching floating offshore wind turbine rotors using frequency-domain Navier-Stokes CFD and blade element momentum theory

To cite this article: A. Ortolani *et al* 2020 *J. Phys.: Conf. Ser.* **1618** 052016

View the article online for updates and enhancements.

Cross-comparative analysis of loads and power of pitching floating offshore wind turbine rotors using frequency-domain Navier-Stokes CFD and blade element momentum theory

A. Ortolani[1], G. Persico[1], J. Drofelnik[2] , A. Jackson[3] and M.S. Campobasso[4]

[1]Dipartimento di Energia, Politecnico di Milano, Via Lambruschini 4, 20156 Milano, Italy
[2]Pipistrel Vertical Solutions d.o.o., Vipavska cesta 2, SI-5270 Ajdovcina, Slovenia

[3]EPCC, University of Edinburgh, Edinburgh EH9 3JZ, UK

[4]Department of Engineering, Lancaster University, Gillow Avenue, LA1 4YW Lancaster, UK

Email: m.s.campobasso@lancaster.ac.uk

Abstract. Reliable predictions of the aero- and hydrodynamic loads acting on floating offshore wind turbines are paramount for assessing fatigue life, designing load and power control systems, and ensuring the overall system stability at all operating conditions. However, significant uncertainty affecting both predictions still exists. This study presents a cross-comparative analysis of the predictions of the aerodynamic loads and power of floating wind turbine rotors using a validated frequency-domain Navier-Stokes Computational Fluid Dynamics solver, and a state-of-the-art Blade Element Momentum theory code. The considered test case is the National Renewable Energy Laboratory 5 MW turbine, assumed to be mounted on a semi-submersible platform. The rotor load and power response at different pitching regimes is assessed and compared using both the high- and low-fidelity methods. The overall qualitative agreement of the two prediction sets is found to be excellent in all cases. At a quantitative level, the high- and low-fidelity predictions of both the mean rotor thrust and the blade out-of-plane bending moments differ by about 1 percent, whereas those of the mean rotor power differ by about 6 percent. Part of these differences at high pitching amplitude appear to depend on differences in dynamic stall predictions of the approaches.

1. Introduction
The increasing amount of R&D efforts in Floating Offshore Wind Turbine (FOWT) technologies stems from the potential of these devices to enable a significantly larger exploitation of wind energy for renewable electricity generation. This is achievable due to the possibility of installing FOWTs further away from the coast, where the wind has higher speed and is often less turbulent than at the offshore sites of current fixed-bottom offshore turbines, and where fixed tower foundations cannot be used due to the technical and economic burden incurred by their use in water depths of 50 meters and more.

However, the durable and profitable operation of FOWTs poses new multi-disciplinary challenges not encountered in the case of fixed-bottom horizontal axis wind turbines [1]. The overall system stability of FOWTs, in fact, is determined by the interaction of a) the hydrodynamic loads on the floater due to surface gravity waves and marine currents, b) the aerodynamic loads on the rotor, nacelle and tower, and c) the restoring loads due to platform mooring lines. Resolving with adequate reliability the physics of each of these load-inducing phenomena is key to the design of the FOWT control and the verification of the overall system damping. Moreover, the development of FOWT wind farms also requires analyzing the generation process [2] and the propagation characteristics [3] of FOWT wakes, which are likely to differ from those of fixed-bottom turbines.

In both the industrial and academic communities, FOWT R&D is often based on the use of low-fidelity engineering codes, such as those implementing the blade element momentum theory (BEMT). These codes were derived and calibrated for fixed-bottom turbine analysis and design. The additional entrainment velocities due to the relatively large FOWT tower motion results in higher and different unsteady aerodynamics of FOWT rotors, and this introduces significant uncertainty in the FOWT analysis making use of legacy low-fidelity aerodynamic codes. To investigate and, ultimately, reduce this uncertainty, several research groups began cross-comparisons of FOWT aerodynamics using low-fidelity codes and high-fidelity Navier-Stokes (NS) Computational Fluid Dynamics (CFD) [4], and these analyses are increasingly becoming of a multi-disciplinary nature [5,6], adopting CFD to resolve both rotor aerodynamics and floater hydrodynamics in a fully coupled fashion.

When using NS CFD for wind turbine aerodynamics, both compressible and incompressible codes can be used. Historically, incompressible codes were used more widely due to their lower computational costs and the fact that the highest relative speeds past turbine rotor did not exceed Mach 0.2. The rapid growth of rotor diameters, however, is prompting more interest in compressible codes [7,8,9], due to the expectation of some that the highest rotor speed of future wind turbines may exceed the Mach 0.2 threshold. In the case of FOWT rotors, the tower entrainment velocities can result in the highest relative air speeds past the blades being well above the compressibility threshold of Mach 0.3, even in the case of rotors which have maximum speeds well below this value when mounted on a fixed-bottom tower. The high speed observed in the FOWT rotor case may result in notable differences between compressible and incompressible flow analyses [2].

This study focuses on the analysis of FOWT rotor aerodynamics, and its main aim is to analyze and discuss the correlation of the predictions a BEMT code and rotor-resolved NS CFD simulations for selected regimes of pitching FOWT rotors. The selected pitching FOWT configuration is the National Renewable Energy Laboratory (NREL) 5MW reference turbine assumed to be mounted on a semi-submersible platform with the same characteristics of that used in [4]. The main objectives of the study are to: a) characterize the dependence of FOWT power and loads on the kinematic parameters of the prescribed harmonic pitching motion, b) assess the amount of nonlinearity in the rotor aerodynamic response to the considered harmonic forcing, and c) analyze and quantify the correlation between the results of the BEMT and NS CFD analyses as the pitching parameters are varied.

2. Computational aerodynamics

The high-fidelity NS CFD code of this study is the Lancaster University COSA compressible code [10], whereas the low-fidelity BEMT code is the NREL open-source AeroDyn BENT code [11], used within the NREL aero-hydro-servo-elastic wind turbine FAST code. Further detail of both simulation set-ups is provided below.

2.1. COSA Harmonic Balance solver

The compressible 3D NS equations are a set of equations expressing the conservation of mass, momentum and energy in a viscous fluid flow. Averaging the NS equations on the turbulence time-scales yields the Reynolds-averaged Navier-Stokes (RANS) equations, which contain an additional term, the Reynolds stress tensor. In the COSA CFD code used in this study, the Reynolds stress tensor is computed with Menter's 2-equation $k - \omega$ shear stress transport SST turbulence model. COSA uses

structured multi-block grids and discretizes the convective fluxes of both the RANS and SST equations with a second order upwind finite volume scheme; it uses second order centered finite differences for both the diffusive fluxes and the space derivatives in the source terms of the SST model. The code can solve rotor flows in both the relative (non-inertial) frame attached to the blades and the absolute (inertial) frame. All COSA FOWT simulations reported herein are performed in the absolute frame of reference.

Several wind turbine flows can be viewed as periodic, and in this circumstance their frequency-domain CFD solution can substantially reduce the analysis runtime with respect to that of the conventional time-domain approach. Nonlinear frequency-domain solution methods of wind turbine flows have been successfully used in several CFD codes [12,13], including COSA [14,15]. Indeed, the harmonic balance (HB) solver has been shown to solve yawed wind turbine flows up to 30 times more rapidly than the standard TD approach with negligible loss penalties in [15], which also reports comprehensive validation of the steady, TD and HB COSA solvers based on the experimental flow measurements of the NREL Phase turbine. In the HB framework, the sought periodic flow is written as a truncated Fourier series retaining only the first few complex harmonics whose frequency is a multiple of the known fundamental frequency of the excitation. The lower runtime of the HB approach is due to the fact that one solves directly for the periodic flow of interest, removing the lengthy time-dependent transient occurring when solving in the TD.

2.2. OpenFAST blade element momentum theory set-up
The low-fidelity simulations of this study use the NREL OpenFAST code in conjunction with the AeroDyn module for solving turbine aerodynamics using BEMT, and the ElastoDyn module for computing the rigid movements and the deformations of the structure. The simulations are carried out using the rigid body model for all system components by disabling all structural flexibility input in ElastoDyn, but enabling the rigid body motion of the platform, as discussed below. The aerodynamic models of AeroDyn allow obtaining the aerodynamic loads acting on both the rotor blades and the turbine tower. Four sub-models are available for turbine aerodynamics, enabling one to account for a) rotor wake induction, b) blade airfoil aerodynamics, c) tower influence on blade aerodynamics, and d) tower drag. The tower is not modelled in this study, and therefore only functionalities a) and b) are used for the low-fidelity results below. To account for the rotor flow unsteadiness due to the FOWT motion, the AeroDyn modelling feature based on the Dynamic Blade Element Momentum Theory (DBEMT), which considers the time-dependence of induction and wake in the balance equations, is adopted. The calculation of the induction factors and resulting inflow velocities and angles relative to the moving blades are based on the local flow field around each analysis node of the considered blade. The effects of local inflow skew, wind shear, turbulence, and tower flow disturbances can also be included in the analysis, but they are not in the present study.

In AeroDyn, Glauert's empirical correction with Buhl's modification replaces the linear momentum balance at high axial induction factors. Three-dimensional flow features are modelled by using Prandtl tip and hub loss corrections and the Pitt-Peters skewed wake correction model. Modelling of airfoil unsteady aerodynamics is accomplished with the Beddoes-Leishman unsteady model, activated by selecting the Minemma-Pierce formulation. This formulation corrects airfoil lift and drag data accounting for trailing and leading edge separations, and dynamic stall. Since in the FOWT simulations below the angles of attack undergo periodic variations and may exceed the static stall limit, the activation of this formulation is essential.

The possible occurrence of a relatively large motion of the whole turbine system, including tower, nacelle and rotor, is a distinctive feature of FOWTs. OpenFAST enables the calculating of the motion of the whole turbine system resulting from the dynamic equilibrium of all loads acting on the turbine, the floater and the mooring lines. In this study, however, the motion of the tower is prescribed, and an ad-hoc procedure has been adopted to enforce the desired tower motion and prevent this from being an output of the analysis. To calculate the motion law of the whole turbine system, OpenFAST imposes its dynamic equilibrium including the aerodynamic loads on rotor and tower, and the hydrodynamic

loads on the floater, restoring loads of the mooring lines and structural loads such as those due to gravity. Mass, damping and stiffness data are required for each component. To incorporate floater dynamics in the analysis, the ExtPtfm input file enables users to assign structural properties and forcing loads at the tower base. To ensure that the tower moves according to the desired law of motion, a two-step process is performed. In the first step, one assigns very high values of mass, rigidity and stiffness to the floating platform, and, applying the equations of dynamic equilibrium of the whole turbine system without aerodynamic loads and using the target tower motion as an input, calculates the forcing loads at the tower basis yielding the desired tower kinematics. The order of magnitude of these loads is very high, due to the adopted high values of the structural properties of the floater. The aerodynamic FOWT analysis is then performed imposing the tower forcing loads obtained in the first step, and using again the set of high values of the structural properties of the floater. This procedure ensures that the aerodynamic forces provide a negligible contribution to the dynamic equilibrium, resulting in the tower moving with the desired motion under the effect of the sole forcing load at the tower base.

3. Rotor grid configuration and CFD set-up

The considered pitching FOWT is based on the NREL 5 MW virtual turbine, which has tower height of 90 m and features a three-blade rotor with diameter of 126 m; the rotor has an overhang of 5 m, a shaft tilt of 5° and pre-coning of 2.5°. Of these three features, only the rotor overhang and tilt have been accounted for in the simulations below.

The rotor geometry and the selected wall boundary conditions are reported in the left schematic of Fig. 1, and the grid around the airfoil at 50 percent tip radius is depicted in the left image of Fig. 1. The outer shape of the physical domain is cylindrical with the rotor center positioned on the cylinder centerline 10 rotor radii from the inlet circular boundary at the front, 20 radii from the outlet circular boundary at the back, and 11 radii from the cylindrical far field boundary. Characteristic far field boundary conditions are enforced on all far field boundaries.

The computational grid has about 10 M cells, and the distance of the first grid nodes off the wall boundaries (blades and hub) from such boundaries results in a y+ value of about 1 in all presented simulations. A butterfly mesh scheme is adopted around the rotor centerline to prevent the formation of degenerate cells. This grid has been shown to deliver mesh-independent solutions in [2], where a finer mesh with about 80 M is used to compute two steady state solutions of the considered rotor. The fine grid was obtained by halving the mesh spacing in all three directions.
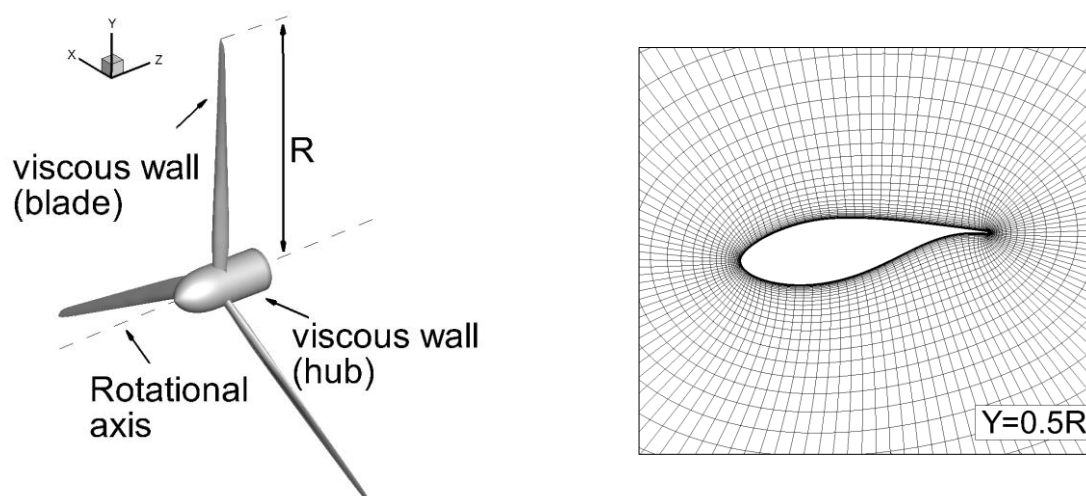

Figure 1. CFD analysis of NREL 5 MW rotor: rotor geometry and wall boundary conditions (left), and airfoil grid at 50 percent tip radius (right).

4. Pitching FOWT configurations

All analyses herein use a close-to-rated wind speed of 11 m/s and a rotor speed of 12 RPM, corresponding to a frequency of 0.2 Hz. The top and front views of the fixed-bottom turbine are depicted, respectively, in the left and middle schematics of Fig.2, along with the orientation of the axes and the positive rotations in the xy plane. The segments labelled B1, B2, B3 denote the blade axes, and the angle θ_r denotes the time-dependent angular position of the reference blade B1, given by $\theta_r = \Omega_r t$, with Ω_r being the rotor angular speed. Since all simulations are carried out in the absolute frame, the position of the xyz Cartesian system, whose origin coincides with the rotor center of the fixed-bottom turbine, does not change during either the fixed-bottom or FOWT analyses presented below. The side view of the considered pitching FOWT is reported in the right schematic of Fig. 2, in which Ω_p denotes the angular frequency of the tower pitching motion. The time-dependent inclination of the tower is $\theta_p = \Theta_p \sin(\Omega_p + \varphi_p)$, where Θ_p is the user-given tower pitching amplitude, and φ_p is the user-given phase between the rotor revolution and the tower pitching, which is constant when Ω_p is an integer multiple of Ω_p. In the FOWT simulations below, $\varphi_p = 0$ and the rotor pitching center is located at the tower base ($y_p = -90$ m) and accounts for the rotor overhang ($z_p = 5$ m). This choice is representative of semi-submersible FOWT platforms.
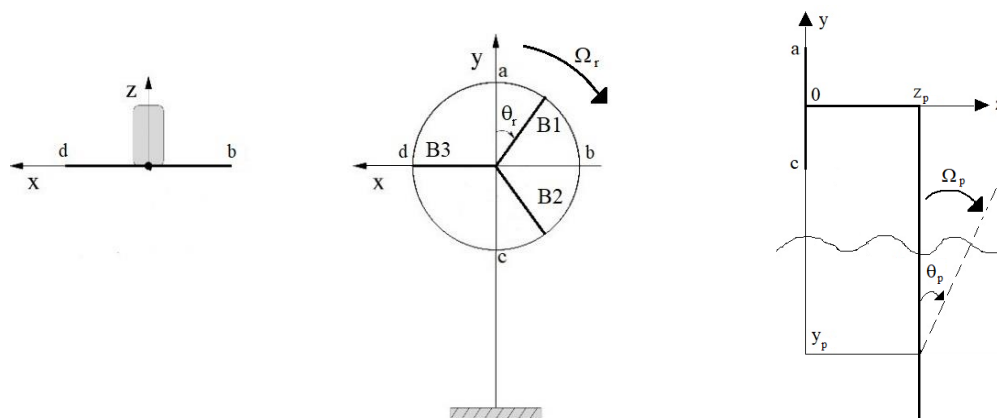

Figure 2. Top view (left schematic) and front view (middle schematic) of fixed-bottom turbine with axis orientation and positive rotation conventions, and side view of FOWT with axis orientation and positive rotations conventions (right schematic).

In the COSA HB NS simulations below, the effect of the rotor tilt has been incorporated by inclining the oncoming wind by 5° upwards on the rotor axis (z axis). Four simulations have been performed. One has motionless tower but is nevertheless unsteady due to the constant 5° misalignment of wind direction and rotor axis. The other three simulations all consider a pitching FOWT with pitching frequency of 0.1 Hz, and have three different pitching amplitudes, namely 1°, 2° and 4°. The selected frequency of 0.1 Hz for the pitching tower is likely to be higher than the pitching eigenfrequency of the floater/turbine system. For example, this eigenfrequency for the OC4 DeepCwind semi-submersible platform mounting the NREL 5 MW turbine considered herein is about 0.038 Hz [16]. The resonant pitching frequency during operation is expected to be higher, although still below 0.1 Hz, due to metocean condition-dependent wind, hydrodynamic and mooring line damping [17]. The pitching frequency of 0.1 Hz has been used in other recent FOWT CFD studies [3,4,5], and, to enable cross-comparison of this study's results with other in the literature, it has been decided to continue using this same frequency.

In the AeroDyn analyses embedded in the OpenFAST analyses, the pre-cone angle of the blades has been removed. and the hub radius has been set to 5 m to make these analyses fully consistent with the CFD simulations. The tilt angle has been assigned in the form of a geometric inclination of the

rotor. The tower pitching motion is enabled by activating the corresponding rigid degree of freedom in ElsatoDyn, and prescribing a forcing load at the tower base determined as described in Section 2.

5. Results

Here, the simulations of COSA and OpenFAST/AeroDyn (named FAST in the remainder of this section for brevity) for different pitching FOWT regimes are cross-compared to a) establish the dependence of the mean, amplitudes and detailed periodic patterns of rotor thrust and power, and blade out-of-plane bending moments on the pitching FOWT regime, and b) analyze the correlation of low- and high-fidelity analyses as the pitching amplitude increases. The COSA harmonic balance solver [14], whose validation was presented in [15], is used for all CFD analyses below. The use of a nonlinear frequency-domain CFD solver, also has the advantage of enabling one to establish the level of nonlinearity due to the flow unsteadiness induced by the platform motion.

5.1. Comparative analysis of rotor thrust and power

The periodic profiles of rotor thrust T and rotor power P obtained with the COSA HB NS simulations and the FAST BEMT analyses for $\Theta_p=1°$, $\Theta_p=2°$ and $\Theta_p=4°$ are reported in Figures 3, 4 and 5 respectively. In each figure, the left plot compares the low- and high-fidelity periodic profiles of the rotor thrust, and the right plot compares those of the rotor power. The variable t/T along the x-axis of all plots is a nondimensionalized time variable used to plot the evolution of the considered output from the start to the end of one pitching cycle, and the symbol T denotes the period of one rotor revolution. The phase φ_p between the rotor revolution and the tower pitching cycle is zero, and therefore $\theta_p= \theta_r=0$ at $t/T=0$ and $t/T=n$, with n being any even integer. All plots report the COSA HB solutions obtained retaining 1, 3 and 4 harmonics in the representation of the sought periodic flow field. It is noted that the difference between the HB3 and HB4 profiles is very small in all cases, indicating that using 3 complex harmonics is sufficient to adequately capture FOWT flow physics at the considered regimes. On the other hand, large quantitative differences exist between the HB1 profiles on one hand and the HB3 and HB4 profiles on the other, indicating a significant level of flow nonlinearity due to rotor pitching even for the fairly small pitching amplitude of 1°.

The agreement between the COSA HB3 and FAST predictions of the thrust profiles is very good at $\Theta_p=1°$ and $\Theta_p=2°$, with the maximum difference of 3.4 percent observed at $t/T=0.16$ for $\Theta_p=2°$. Interestingly, at $\Theta_p=1°$ and $\Theta_p=2°$, the largest discrepancies between the two predictions occur in the first 25 percent of the pitching cycle ($0<t/T<0.5$), the interval corresponding to the retreating part of the pitching trajectory, a phase in which rotor/wake interactions are more pronounced. The different approach of the two codes to resolving these interactions is thus likely to account for the differences between the thrust profiles in this part of the cycle. The comparison of the low- and high-fidelity power profiles at $\Theta_p=1°$ and $\Theta_p=2°$ is qualitatively similar to that discussed for the thrust profiles, although the power differences are slightly higher than the thrust differences, with the maximum power difference of 12.5 percent occurring at $t/T=0.12$ for $\Theta_p=2°$. It is also observed that the agreement of the power profiles in the interval $1.2<t/T<1.6$, which corresponds to a significant portion of the windward pitching trajectory, improves moving from $\Theta_p=1°$ to $\Theta_p=2°$. A possible reason for this is that the forward speed of the rotor increases with Θ_p, and rotor/wake interactions will tend to decrease in the windward trajectory of the FOWT, as the forward speed increases.

At $\Theta_p=4°$ a qualitative change in the trends discussed above is noted. In the interval $0.8<t/T<1.3$ the FAST thrust and power curves flatten out more rapidly than their COSA HB3 counterparts, and this results in larger discrepancies between the CFD and BEMT predictions in this region of the pitching cycle, corresponding to the highest windward entrainment speeds of the tower. In this condition, the angle of attack perceived by the blades may increase significantly and result in stall, reducing blade lift and, in turn, rotor torque and thrust. The power difference of about 1 MW at $t/T=1$ between BEMT and CFD predictions is due to the fact that the CFD simulation does not predict the same level of stall of the BEMT method, whose prediction is quite sensitive to correlation and semi-analytic models, such as corrections for 3D flow effects and dynamic stall models. In field applications the blade pitch

control is likely to prevent the occurrence of very high angles of attack due to tower pitching, but this is a condition that may occur in extreme cases, such as sudden faults of the blade pitch actuation.
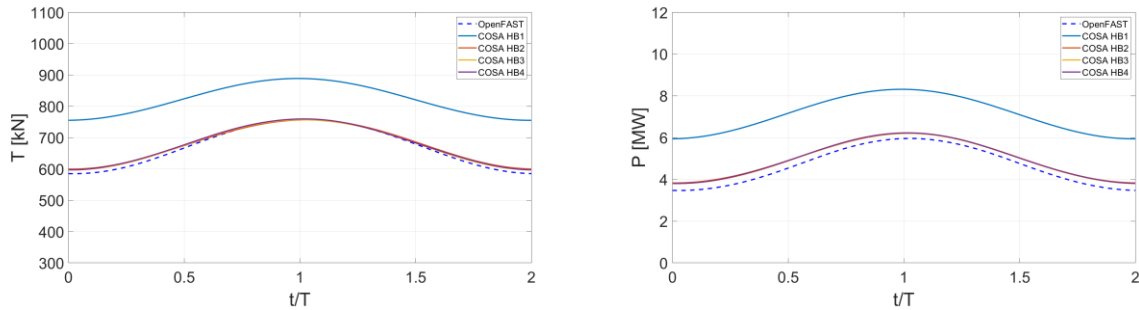

Figure 3. COSA harmonic balance and OpenFAST/AeroDyn predictions of periodic profiles of thrust T (left) and power P (right) of pitching NREL 5 MW rotor at $\Theta_p=1^\circ$.
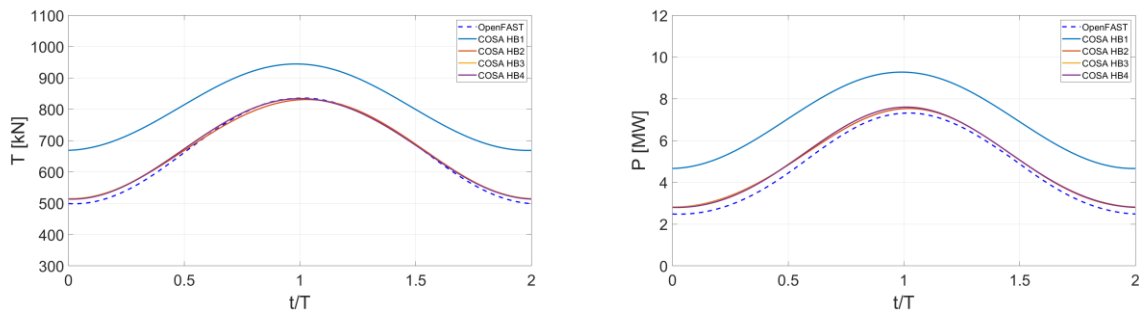

Figure 4. COSA harmonic balance and OpenFAST/AeroDyn predictions of periodic profiles of thrust T (left) and power P (right) of pitching NREL 5 MW rotor at $\Theta_p=2^\circ$.
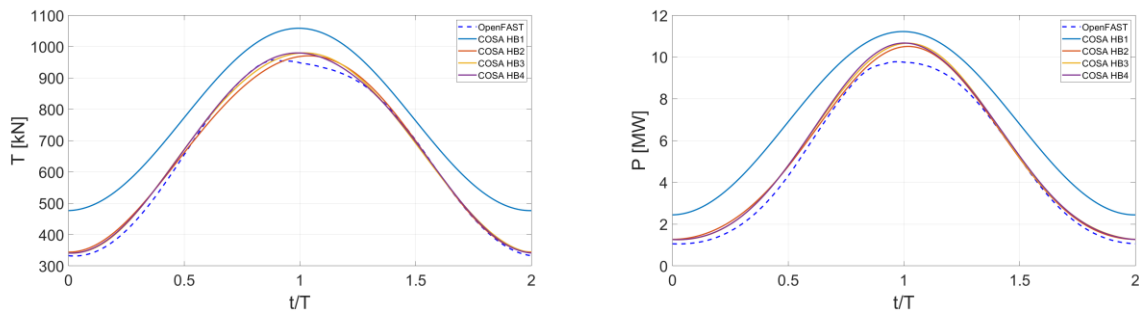

Figure 5. COSA harmonic balance and OpenFAST/AeroDyn predictions of periodic profiles of thrust T (left) and power P (right) of pitching NREL 5 MW rotor at $\Theta_p=4^\circ$.

To provide more quantitative and engineering practice-relevant estimates of how the agreement between CFD and BEMT FOWT rotor performance and load predictions vary with the severity of the pitching regime, the mean and the maximum values of the T and P computed with the two methods are reported in Tables 1 and 2 respectively. In both tables, the fifth row also provides the percentage difference of the high- and low-fidelity predictions. For reference, the second and third columns of both tables also report the analysis results for the fixed-bottom counterpart of the three FOWT regimes discussed so far. The results of the mean outputs presented in Tab. 1 show that the difference of mean thrust of the two codes is about 1 percent in all four turbine operation modes, whereas that of mean power is about 6 percent, and is maximum at $\Theta=4^\circ$, due to the differences in stall prediction.

Table 2 highlights that the CFD and BEMT predictions of the maximum values of rotor thrust and power for the fixed-bottom turbine and the FOWT with pitching amplitudes $\Theta_p=1°$ and $\Theta_p=2°$ differ by amounts similar to those observed for the mean output analysis in Tab. 1. At $\Theta_p=4°$, however, the percentage differences of maximum rotor and thrust grow significantly due to the higher detrimental impact of stall predicted by the BEMT analysis.

Table 1. COSA HB3 and OpenFAST/AeroDyn mean values of rotor thrust T [KN] and rotor power P [MW] for examined fixed-bottom and pitching FOWT cases.

	Fixed-bottom		FOWT: $\Theta_p=1°$		FOWT: $\Theta_p=2°$		FOWT: $\Theta_p=4°$	
	T	P	T	P	T	P	T	P
FAST	672.6	4.64	672.3	4.68	670.4	4.78	661.2	5.11
COSA	678.4	4.94	677.8	4.97	676.8	5.07	670.9	5.48
Δ (%)	0.85	6.07	0.81	5.84	0.95	5.72	1.45	6.75

Table 2. COSA HB3 and OpenFAST/AeroDyn peak values of rotor thrust T [KN] and rotor power P [MW] for examined fixed-bottom and pitching FOWT cases.

	Fixed-bottom		FOWT: $\Theta_p=1°$		FOWT: $\Theta_p=2°$		FOWT: $\Theta_p=4°$	
	T	P	T	P	T	P	T	P
FAST	672.7	4.64	758.3	5.96	835.8	7.32	957.8	9.78
COSA	679.7	4.95	766.7	6.21	834.2	7.61	980.0	10.7
Δ (%)	1.03	6.26	1.10	4.03	-0.19	3.81	2.27	8.60

5.2. Comparative analysis of blade out-of-plane bending moment

The out-of-plane bending moment (BM) of all three blades predicted by the COSA HB3 and HB4 analyses and the FAST simulations at $\Theta_p=1°$, $\Theta_p=2°$ and $\Theta_p=4°$ are depicted in Figures 6, 7 and 8 respectively. The considered BM is calculated with respect to the axis contained in the rotor plane, normal to the blade axis and passing through the rotor center. The blade counting indicated in all three figures is that adopted in the middle schematic of Fig. 2. As $\Omega_r=2\Omega_p$ and $\varphi_p=0°$, the maximum BM of all blades always occurs at $t/T=1$, when the tower is upright and its top has maximum windward velocity. For each FOWT regime, the maximum BM is experienced by blade 1, since this blade always experiences the highest tower-induced entrainment velocity and angles of attack at $t/T=1$. A cross-comparison of the periodic BM profiles in Figures 6, 7 and 8 highlights that while the mean value of the blade BM does not vary significantly as Θ_p increases, its variation over the pitching cycle increases significantly with the pitching amplitude. For example, the variation of BM1 doubles moving from $\Theta_p=1°$ to $\Theta_p=2°$, an occurrence which has a significant impact on FOWT design with respect to fatigue loads.

At all considered pitching amplitudes, the BM predictions of the FAST and COSA HB analyses are in very good agreement, although the estimates of the former analyses are marginally higher than those of the CFD predictions. One also notes that some small differences also exist between the COSA HB3 and HB4 BM profiles, which are larger than the differences between the HB3 and HB4 profiles of rotor thrust and power examined in Figures 3, 4 and 5. A possible cause for the small mismatch of the BM profiles obtained with the HB3 and HB4 solutions could be that more harmonics may be required to achieve a harmonic-independent estimate of this variable.
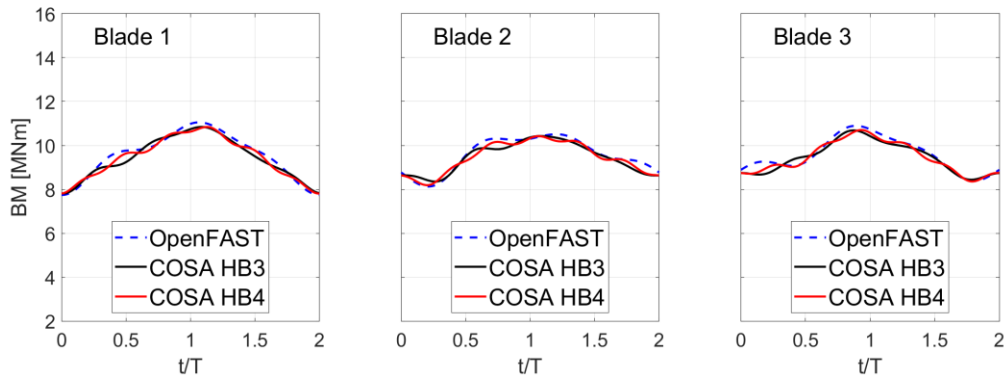
Figure 6. COSA harmonic balance and OpenFAST/AeroDyn predictions of periodic profiles of the out-of-plane bending moment BM on the blades of the pitching NREL 5 MW rotor at $\Theta_p=1^o$.
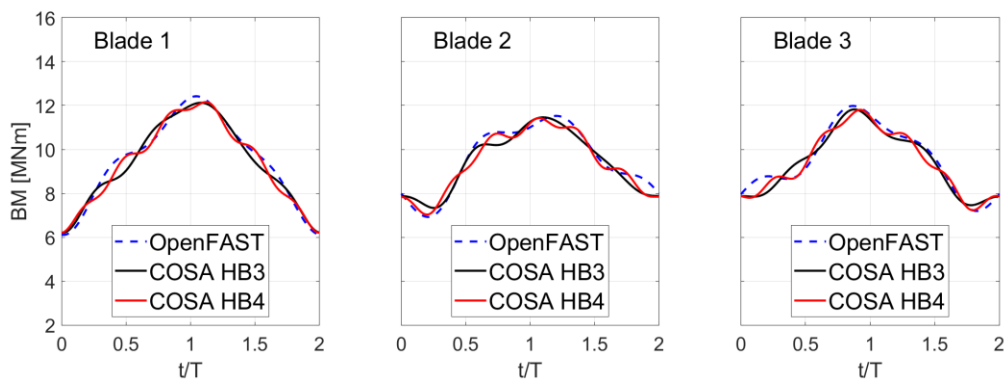

Figure 7. COSA harmonic balance and OpenFAST/AeroDyn predictions of periodic profiles of the out-of-plane bending moment BM on the blades of the pitching NREL 5 MW rotor at $\Theta_p=2^o$.
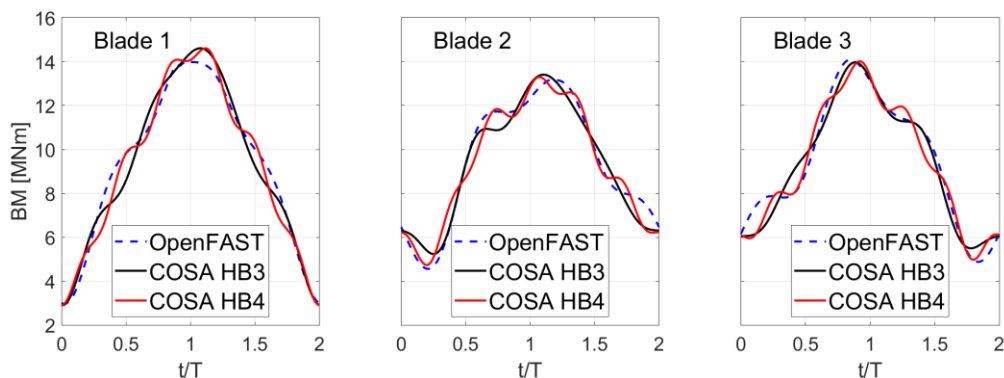

Figure 8. COSA harmonic balance and OpenFAST/AeroDyn predictions of periodic profiles of the out-of-plane bending moment BM on the blades of the pitching NREL 5 MW rotor at $\Theta_p=4^o$.

A quantitative comparison of the blade out-of-plane bending moment obtained with the CFD and BEMT-based analyses is provided in Tables 3 and 4. The third and fourth rows of the former table provide the mean value of BM of all blades at all examined pitching amplitudes obtained with FAST and COSA HB3 analyses, respectively, whereas the data of the third and fourth rows of the latter table provide the maximum values of the same variable obtained with the two aforementioned analyses. For reference purpose, the second and third columns of both tables also report the analysis results for the fixed-bottom counterpart of the three examined FOWT regimes. In both tables, the fifth row provides the percentage difference of the high- and low-fidelity predictions. The data of Tab. 3 confirm that

both low- and high-fidelity analyses predict a very low sensitivity of the mean bending moments to the pitching amplitude of the tower, while those of Tab. 4 indicate a strong dependence of the amplitude of the periodic variation of BM on Θ_p. The data of the row of percentage errors show that mean values of the CFD and BEMT analyses differ by about 1 percent and the peak values by about 2 percent.

Table 3. COSA HB3 and OpenFAST/AeroDyn mean values of out-of-plane bending moment BM [MNm] of all blades for examined fixed-bottom and pitching FOWT cases.

	Fixed-bottom			FOWT: Θ_p =1º			FOWT: Θ_p =2º			FOWT: Θ_p =4º		
	BM1	BM2	BM3	BM1	BM2	BM3	BM1	BM2	BM3	BM1	BM2	BM3
FAST	9.59	9.59	9.59	9.58	9.58	9.59	9.53	9.53	9.57	9.34	9.45	9.51
COSA	9.46	9.46	9.46	9.45	9.46	9.46	9.43	9.46	9.46	9.30	9.40	9.42
Δ (%)	-1.37	-1.37	-1.37	-1.38	-1.27	-1.37	-1.06	-0.74	-1.37	-1.37	-1.37	-1.38

Table 4. COSA HB3 and OpenFAST/AeroDyn peak values of out-of-plane bending moment BM [MNm] of all blades for examined fixed-bottom and pitching FOWT cases.

	Fixed-bottom			FOWT: Θ_p =1º			FOWT: Θ_p =2º			FOWT: Θ_p =4º		
	BM1	BM2	BM3	BM1	BM2	BM3	BM1	BM2	BM3	BM1	BM2	BM3
FAST	9.84	9.84	9.84	11.05	10.51	10.89	12.42	11.53	11.98	14.04	13.17	14.08
COSA	9.60	9.60	9.61	10.84	10.42	10.69	12.13	11.46	11.82	14.61	13.41	13.97
Δ (%)	-2.50	-2.50	-2.39	-1.94	-0.86	-1.87	-2.39	-0.61	-2.50	-2.50	-2.39	-1.94

For both the fixed-tower and the pitching rotor cases, the results of Tables 1-4 show a good agreement of low- and high-fidelity predictions in terms of rotor thrust and blade BMs, and slightly larger relative differences of rotor power data. This is possibly due to differences of the axial induction predicted at the rotor position by COSA and AeroDyn, caused, in turn, by different modelling/simulation approaches, such as a semi-empirical tip loss correction independent of the actual blade tip geometry with BEMT, and a complete 3D tip flow field resolution with CFD. Using steady analyses does not alter qualitatively the aforementioned differences of BEMT and CFD results. The comparison of the steady COSA/AeroDyn fixed-bottom turbine analyses of the NREL 5 MW rotor without shaft tilt [6] shows excellent power agreement but higher AeroDyn thrust. This indicates that the BEMT/CFD differences for the FOWT rotor with both small and high amplitudes are also due to differences in the unsteady flow modelling/simulation features of the two approaches, with some indication that further analysis of the present formulation/implementation of the Beddoes-Leishman model may be needed.

6. Conclusions

A cross-comparative analysis of a pitching FOWT rotor based on the BEMT functionalities embedded in the OpenFAST code, and the COSA harmonic balance NS CFD code has been presented. Here, the NREL 5 MW turbine rotor at close-to-rated wind speed and subject to pitching amplitudes of 1, 2 and 4 degrees with pitching frequency of 0.1 Hz is considered. The overall correlation of BEMT and CFD results is quite good, with estimates of rotor thrust and blade out-of-plane bending moments differing by about 1 percent, and rotor power by up to 6 percent. The largest differences between the predictions of the two approaches are found at the largest pitching amplitude, due to differences in the prediction of the detrimental effects of dynamic stall. These effects are more pronounced in the BEMT analysis.

Both BEMT and CFD methods predict a fairly low sensitivity of the mean rotor thrust and blade bending moments to the pitching amplitude, but a quite high sensitivity of the amplitude of the periodic variations of these two loads. Both methods predict that the increment of the amplitude of the blade bending moments with the tower pitching amplitude is notably higher than the increment of the amplitude of the rotor thrust, a trend expected on the basis of fundamental wind turbine aerodynamics.

References
[1]   Sebastian T and Lackner M A S 2018, Characterization of the unsteady aerodynamics of offshore floating wind turbines, *Wind Energy*, **16**(3): 339-352.
[2]   Ortolani A, Persico G, Drofelnik J, Jackson and Campobasso M S 2020, High-fidelity calculation of floating offshore wind turbines under pitching motion, *ASME Turbo Expo Technical Congress and Exposition*, ASME paper GT2020-15552.
[3]   Lienard C, Boisard R and Daudin C 2019, Aerodynamic behavior of a floating offshore wind turbine, *AIAA SciTech Forum*, American Institute of Aeronautics and Astronautics.
[4]   Tran T-T and Kim D-H 2015, The platform pitching motion of floating offshore wind turbine: a preliminary unsteady aerodynamic analysis, *J. wind eng. ind. Aerody.*, **142**: 65-81.
[5]   Tran T-T and Kim D-H 2016, Fully coupled aerohydrodynamic analysis of a semi-submersible FOWT using a dynamic fluid body interaction approach, *Renewable Energy*, **92**: 244-261.
[6]   Liu Y, Xiao Q, Incecik A, Peyrard C, Wan D 2017, Establishing a fully coupled CFD analysis tool for floating offshore wind turbines, *Renewable Energy*, **112**: 280-301.
[7]   Campobasso M S, Yam M, Drofelnik J, Piskopakis A and Caboni M 2014, Compressible Reynolds-averaged Navier-Stokes analysis of wind turbine turbulent flows using a fully coupled low-speed preconditioned multigrid solver, *ASME Turbo Expo Technical Congress and Exposition*, ASME paper GT2014-25562.
[8]   Yan C and Archer C L 2018, Assessing compressibility effects on the performance of large horizontal axis wind turbines, *Applied Energy*, **212**: 35-45.
[9]   Sørensen N N, Bertagnolio F, Jost E and Lutz T 2018, Aerodynamic effects of compressibility for wind turbines at high tip speeds, *J. Phys.: Conf. Ser.* **1037** 022003.
[10]   Campobasso M S, Piskopakis A, Drofelnik J, Jackson A 2013, Turbulent Navier-Stokes analysis of an oscillating wing in a power extraction regime using the shear stress transport turbulence model*, Computers and Fluids*, **88**: 136-155.
[11]   Heyman G, Jonkman B, Murray R, Damiani R, and Jonkman J 2019, AeroDyn: a time-domain wind and MHK turbine aerodynamics module, *National Renewable Energy Laboratory.* https://nwtc.nrel. gov/AeroDyn. Accessed on 28 February 2020.
[12]   Horcas S G, Debrabandere F, Tartinville B, Hirsch C and Coussement G 2017, Rotor-tower interactions of DTU 10 MW reference wind turbine with a non-linear harmonic method, *Wind Energy*, **20**(4): 619-636.
[13]   Howison J and Ekici K 2015, Dynamic stall analysis using harmonic balance and correlation based γ-Re$_\theta$ transition model for wind turbine applications, *Wind Energy*, **18**(12): 2047-2063.
[14]   Campobasso M S and Baba-Ahmadi M H 2012, Analysis of Unsteady Flows Past Horizontal Axis Wind Turbine Airfoils Based on Harmonic Balance Compressible Navier-Stokes Equations with Low-Speed Preconditioning, *J. Turbomach.*, **134**(6): 061020-061032.
[15]   Drofelnik J, Da Ronch A and Campobasso M S 2018, Harmonic balance Navier-Stokes aerodynamic analysis of wind turbines in yawed wind, *Wind Energy*, **21**(7): 515-530.
[16]   Coulling A J, Goupee A J, Robertson A N, Jonkman J M, and Dagher H J 2013, Validation of a FAST semi-submersible floating wind turbine numerical model with DeepCwind test data, Journal of Renewable and Sustainable Energy **5**(2) 023116.
[17]   Pham T D and Shin H 2019, A New Conceptual Design and Dynamic Analysis of a Spar-Type Offshore Wind Turbine Combined with a Moonpool, *Energies*, **12**(19) 3737.